Journal of Power Sources 206 (2012) 463–468

Contents lists available at SciVerse ScienceDirect

Journal of Power Sources

journal homepage: www.elsevier.com/locate/jpowsour

Using eggshell membrane as a separator in supercapacitor

Haijun Yu, Qunwei Tang, Jihuai Wu*, Youzhen Lin, Leqing Fan, Miaoliang Huang, Jianming Lin, Yan Li, Fuda Yu

Engineering Research Center of Environment-Friendly Functional Materials, Ministry of Education, Institute of Materials Physical Chemistry, Huaqiao University, Quanzhou 362021, China

ARTICLE INFO

Article history:
Received 18 October 2011
Received in revised form 16 January 2012
Accepted 18 January 2012
Available online 28 January 2012

Keywords:
Eggshell membrane
Supercapacitor
Separator
Stability

ABSTRACT

A separator is prepared based on natural and flexible eggshell membrane (ESM) for supercapacitor application. Morphology observation shows that the ESM is consisted of hierarchically ordered macroporous network. With a high decomposition temperature (>220 °C), enough mechanical strength (σ_{max} = 6.59 ± 0.48 MPa, ε_{max} = 6.98 ± 0.31%, respectively), and low water uptake and swelling property (<10%), ESM could be a promising candidate for supercapacitor separator. As expected, the supercapacitor with ESM separator exhibits outstanding electrochemical performances, such as low resistance, quick charge–discharge ability (τ is 4.76 s), and good cyclic stability (92% retention after 10,000 cycles). However, the one with PE separator shows worse properties (high resistance, low specific capacitance, etc.). This research provides new insight into the preparation of natural, low-cost and high-performance separator for supercapacitor and other applications.

1. Introduction

In recent years, great efforts have been devoted to the development of alternative energy storage/conversion devices in response to the depletion of fossil fuels and related environmental issues [1–3]. Supercapacitor, also known as electrochemical capacitor or double electric layer capacitor, is an important energy-storage device, which has attracted increasing attentions because of its high power density, long cycle life, and environment-friendly feature [4–7]. One of the key questions about designing high-performance supercapacitor is the choice of separators [8]. In particular, the utilization of high-surface-area electrodes and the high-efficient electrolytes in supercapacitors have aroused intense researches on separators. Separators used between electrodes in supercapacitor have been constructed of rubber, plastic, aquagel, resorcinol formaldehyde polymers, polyolefin films, etc. to prevent the conduction of electrons between the electrodes, but such prior known separators have had a tendency to dry out or collapse over a period of time, or exhibit poor ionic conductivity [9–11]. Consequently, a need exists for supercapacitor separators, which are made of highly porous materials that provide minimal resistance for electrolyte ion's movement and that at the same time, have electronic insulator properties between opposing electrodes.

Now, the most common separator used in commercial supercapacitors is Nafion membrane, which is composed of a hydrophobic Teflon backbone and side chains terminated with hydrophilic sulfonic acid (—SO_3H) groups [12,13]. Although Nafion membrane employs efficient properties for the role of supercapacitor separator, the expensive spend and limited raw materials from fossil resources limits the large-scale application of supercapacitors [14–16]. In other words, although the industrialization of Nafion membrane can be realized at acceptable cost in the foreseeable future, it fails to meet the requirements of the development of low-carbon society. Thus, it is very valuable and significative to develop natural membrane materials with excellent properties for supercapacitors.

It is known that avian eggshells are formed by layered organization of calcified shell and organic ESM containing collagen types I, V, and X, and glycosaminoglycans [17]. ESMs are consisted of the outer shell membrane, inner shell membrane, and limiting membrane surrounding the egg white. The outer shell membrane, which can be easily isolated from eggshells, was used as separate for supercapacitors in this work. ESM can keep good stability in aqueous and alcoholic media and undergo pyrolysis on heating [18]. Furthermore, it is actually the most abundant material in biosphere with non-toxicity and low-cost properties. So our present work can be regarded as a novel attempt to utilize a natural membrane to alternate the conventional polymer separator derived from oil resources.

2. Experimental

2.1. Materials and reagents

Activated carbon material was supplied by Shanghai Heda carbon Co., Ltd. (nitrogen BET surface area of 1900 $m^2 g^{-1}$) and

* Corresponding author. Tel.: +86 595 22692229; fax: +86 595 22692229.
E-mail address: jhwu@hqu.edu.cn (J. Wu).

0378-7753/$ – see front matter © 2012 Elsevier B.V. All rights reserved.
doi:10.1016/j.jpowsour.2012.01.116

used as received without further treatments. Polytetrafluoroethylene (PTFE) and nickel foil were purchased commercially from Guangzhou Xingshengjie Co. Ltd. and Changsha Lyrun new material Co. Ltd., respectively. Graphite, sodium sulfate (Na_2SO_4), N-methyl-2-pyrrolidone (NMP), and polypropylene (PP, 0.9 mm) were commercially available materials from Sinopharm Chemical Reagent Co., Ltd. and used without further treatments.

2.2. Separation of ESM

The separation of the outer shell membrane from eggs has been described previously [19]. Briefly, eggs were gently broken and emptied via the blunt end. The eggshells were washed with deionized water and then the inner shell membrane and the limiting membrane were manually removed. The remaining eggshells were immersed in 1 mol L^{-1} HCl aqueous solution to dissolve the $CaCO_3$ shell, leaving the organic outer shell membrane. After the outer shell membrane was washed with water thoroughly, the resultant ESM (0.8 mm) was prepared for supercapacitor applications.

2.3. Characterizations

The morphological structure of ESM was observed and photographed by an S-4700 Hitachi cold field emission scanning electron microscopy (SEM). Thermal gravimetric analysis (TGA) of the samples was performed on TA make a TGA 2050 instrument to monitor the degeneration temperature of ESM. The experimental procedure consisted of heating the samples in flowing nitrogen (99.999% purity, 100 mL min^{-1}) at a linear heating rate of 15 °C min^{-1} from room temperature to 750 °C until all the samples were completely consumed.

The tensile strength–elongation test of the ESM and PP were carried out on an INSTRON Model 5583 testing machine (USA) by following the procedure reported in our previous research [20]. The test conditions were controlled as follows: the temperature was set at 25 °C, the size of humid sample was cut with a knife to 2 mm × 10 mm, the distance between two square panels was 5 mm, and the crosshead speed was 5 mm min^{-1}. The thickness of the membrane was ~100 μm from SEM observation. Since the thickness of the ESM was not perfectly uniform, it was average to a yield of 100 μm from measurements at more than 20 points along the horizontal direction of each sample. The strain under stress is defined as the change in length relative to the initial length of the specimen. The tensile strength and strain at break were calculated on the basis of the initial cross-section area. For each set of data, more than 5 samples were prepared and measured at identical conditions. Each data set showed similar stress–strain behavior. As an average, from each measurement one typical data set was selected.

2.4. The properties of water uptake and swelling

The dry membrane was weighted (W_{dry}) and immersed in 1 mol L^{-1} Na_2SO_4 solution for different days at room temperature to reach certain dilation, respectively. And then the membrane was taken out of the solution and carefully wiped with an absorbent paper before it was weighed (W_{wet}). The swelling was determined in a similar method, by soaking the dry rectangular membrane (about 1.0 cm × 1.0 cm) with area of A_{dry} in 1 mol L^{-1} Na_2SO_4 solution for different days, then re-measuring to obtain the wetted membrane area (A_{wet}). The degree of water uptake (D_w) and swell (D_s) were determined from the differences between the wet and dry membranes according to equation [21,27]:

$$D_w = \frac{W_{wet} - W_{dry}}{W_{dry}} \times 100\% \quad (1)$$

$$D_s = \frac{A_{wet} - A_{dry}}{A_{dry}} \times 100\% \quad (2)$$

2.5. Fabrication of activated carbon electrodes

The electrodes for supercapacitors were composed of 85 wt.% activated carbon, 10 wt.% graphite, and 5 wt.% PTFE [22]. The activated carbon and graphite powders were added to PTFE/NMP mixture and the mixture was stirred to form carbon slurry at room temperature. And then the carbon slurry was pressed by Decal method to form a thin sheet. Under pressure of 10 MPa, the sheet was painted on nickel foam that acts as the current collector. After being dried at 60 °C for 24 h in a vacuum, an as-prepared electrode was obtained.

2.6. Assembly and measurements of supercapacitors

Two as-prepared activated carbon electrodes fitted with the ESM separator and electrolyte solution constitute a classical Swagelok®-type cell [23]. Before assembling the supercapacitor configuration, activated carbon electrodes and ESM were immersed in 1 mol L^{-1} Na_2SO_4 electrolyte for 24 h to make aqueous electrolyte solutions homogeneously diffuse into the pores of carbon electrodes. As comparison, the supercapacitor based on PP separator and the same electrolyte was assembled.

Electrochemical measurements were performed on an electrochemical workstation system (CHI 660C, Shanghai ChenHua Co., Ltd.). Cyclic voltammetry (CV), electrochemical impedance spectroscopy (EIS) and galvanostatic charge–discharge (GCD) measurements were determined to evaluate the performances of the supercapacitor. The supercapacitor specific capacitance (C, F g^{-1}) and single-electrode specific capacitance (C_s, F g^{-1}) were evaluated from charge–discharge curves according to the following equation [24,25]:

$$C = \frac{I \times \Delta t}{\Delta V \times m_{ac}} \quad (3)$$

$$C_s = 4 \times C \quad (4)$$

where I (A) is the discharge current, m_{ac} (g) is the weight of active material (including the binder and the graphite), Δt (s) is the charge–discharge time, ΔV (V) represents the actual voltage excluding iR_{drop} of the discharge process. Besides, the coulombic efficiency (η) was evaluated using the following relation, when the same current is used for charging and discharging [26]:

$$\eta = \frac{t_d}{t_c} \times 100\% \quad (5)$$

where t_c (s) and t_d (s) are the charging and discharging times, respectively.

3. Results and discussion

3.1. Morphology observation

The typical SEM images of the natural ESM were shown in Fig. 1. One can see that the membrane is a macroporous network composed of interwoven and coalescing shell membrane fibers ranging in diameter from 0.5 to 1 μm. The presence of macropores with pore sizes of 1–3 μm is evident, providing a superhigh way for diffusing ions with a low resistance so as to enhance the performance of supercapacitors [27].

3.2. Thermal stability and mechanical strength

High thermal stability and excellent mechanical strength in a separator are prerequisites to obtain high-performance

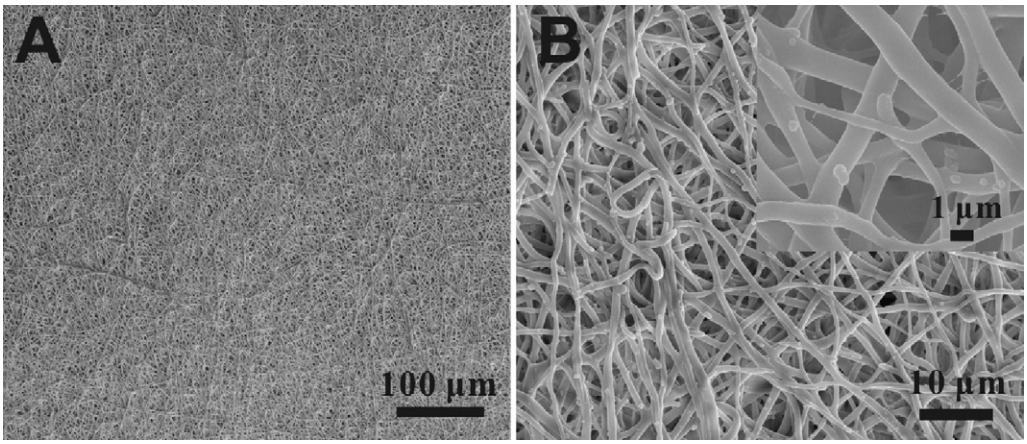

Fig. 1. SEM photographs of ESM at low (A) and high (B) magnifications.

Table 1
The decomposition temperatures, maximum stress and strain of the ESM.

Tests	TGA		Mechanical strength (average ± standard deviation)	
Parameters	Starting decomposition temperature (°C)	Complete decomposition temperature (°C)	Maximum stress (σ_{max}) (MPa)	Maximum strain (ε_{max}) (%)
Values	215	541	6.59 ± 0.48	6.98 ± 0.31

supercapacitors. The thermal stability of the ESM was analyzed by TGA experiments in a nitrogen-containing atmosphere, and the TGA thermograms and decomposition temperatures were presented in Fig. 2A and Table 1. The ESM would undergo three-step weight loss stage as follows: (i) water evaporation from membrane phase around 50–100 °C; (ii) degradation of collagen and glycans chains around 220–400 °C; (iii) final membrane matrix degradation around 400–650 °C, which is consistent with previous study [28]. Compared with PP membranes, for which the degradation of the structural groups occurs at a similar temperature (about 245 °C) [29], ESM matrix began to degrade at approximately 220 °C. This indicates that the membrane could retain its good properties at practical operating temperatures (<100 °C) and even at high temperatures (>100 °C) for supercapacitor applications.

Fig. 2B presented the tensile stress–strain (σ-ε) curve of the ESM, and the σ_{max} and ε_{max} are also listed in Table 1. One can see that there was a good correlation between the breaking stress and breaking strain because the tensile stress increased dramatically in the larger strain region. The σ_{max} and ε_{max} of ESM were 6.59 ± 0.48 MPa and 6.98 ± 0.31%, respectively. As comparison, the mechanical strength test of conventional PP separator was measured and the results were also presented in Fig. 2B. We can see that the mechanical property of PP membrane is a little better than ESM membrane, which are usually as the separator for supercapacitor [30,31]. From the point of view of the practical application, ESM with such mechanical strength can be regarded as a potential separator for the supercapacitor applications.

3.3. Water uptake and swelling

In order to investigate the long-term stability of ESM, the water uptake and swelling of ESM were determined by immersed in 1 mol L^{-1} Na_2SO_4 aqueous solution at room temperature. Here, we monitored the mass and areas changes of the sample after different storage times to evaluate the stability of ESM, using the mass of the ESM (W_{dry}) after dry at 80 °C for 12 h as standards. The changes in weight and area were monitored and the D_w and D_s were calculated according to Eqs. (1) and (2), which were presented in Fig. 3.

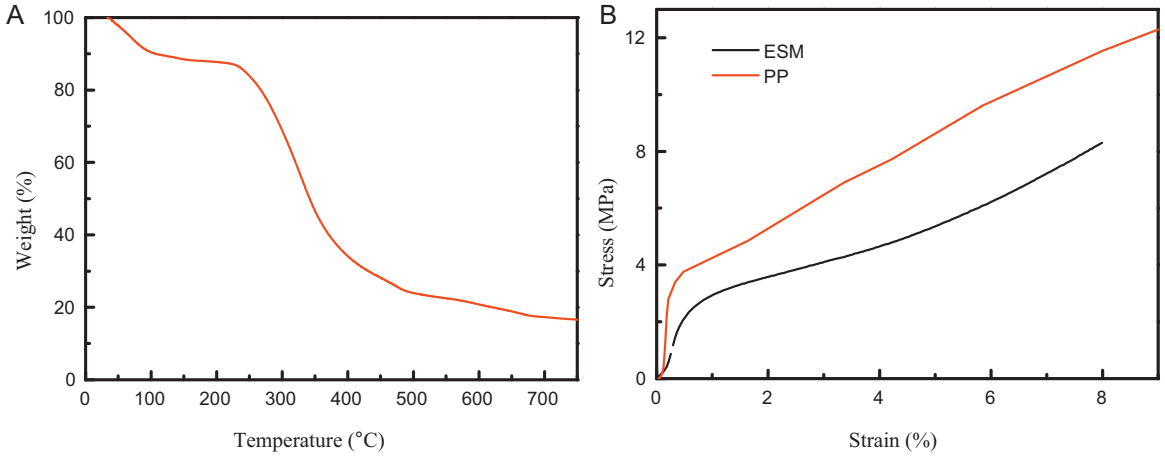

Fig. 2. (A) TGA thermodiagram of the ESM and (B) tensile stress–strain curves of the ESM and PP.

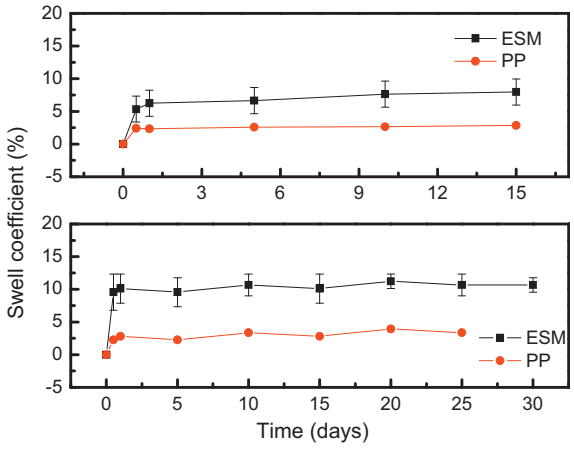

Fig. 3. Time courses of coefficient (%) for ESM and PP in 1 mol L^{-1} NaS_2O_4 aqueous solution at room temperature.

At the same time, the water uptake and swelling of PP were also determined and the results were shown in Fig. 3. To some extent, the ESM will swell in 1 mol L^{-1} Na_2SO_4 aqueous solution because of the decoration of hydrophilic groups such as —COOH and —NH_2 on the backbone of ESM. From Fig. 3, one can see that the D_w and D_s are in a very low level, keeping around 10% and 8%, respectively. Obviously, the D_w and D_s of PP membrane are about 3%, which are ascribed to the low wettability of the membrane. It is well-known that water uptake and swelling property are important parameters in view of electrochemical applications [27]. The low water uptake and swelling degrees of an ESM indicate a potential candidate for the separator of supercapacitors.

3.4. Electrochemical performances of supercapacitors

In order to evaluate the charge–discharge response of the supercapacitors, CV measurements were conducted under a range of scan rates. Fig. 4A shows the CV curves obtained with potential scan rates ranging from 5 to 100 mV s^{-1} for a symmetric supercapacitor with ESM separator. The unique rectangular shape revealed that the charge was accumulated at the electrolyte/electrode interface through an electric double layer. The CV curve still retains a relatively rectangular shape without obvious distortion with the increase of scan rates from 5 mV s^{-1} to 100 mV s^{-1}, demonstrating excellent high-rate performance. High-rate performance of supercapacitor is not only attributed to the low contact restitance between the electrodes, current collector and the separator, but also ascribed to the superhighway for diffusing ions that provided by the separator, which has been interpreted aforementioned. Besides, the CV tests of supercapacitor employing conventional PP separator were characterizated and results as shown in Fig. 3B. From Fig. 3B, we can see that the CV curves of supercapacitor with PP separator exhibits obvious distortion at the scan rate of 15 mV s^{-1}, but the CV shapes of supercapacitor with ESM separator are nearly a rectangular at the same sweep rate, which indicates the

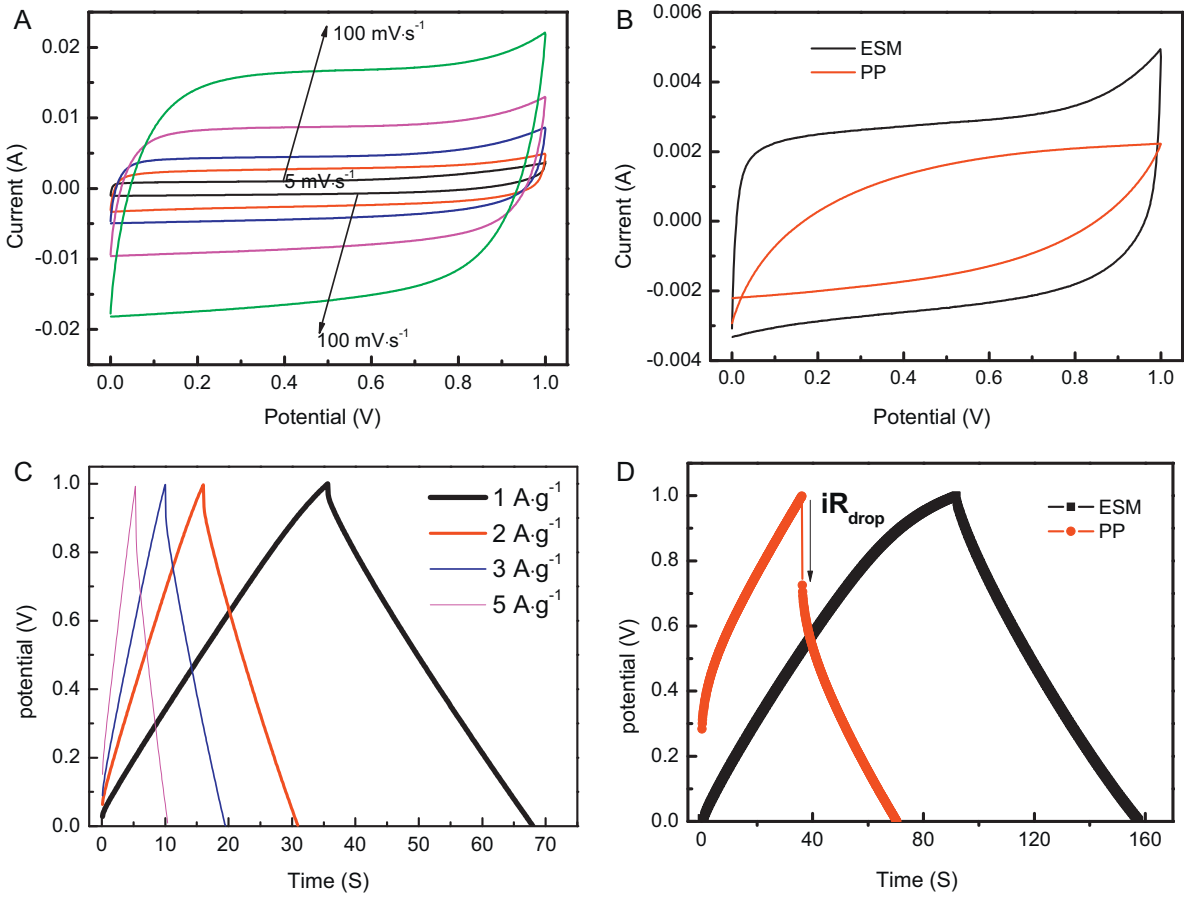

Fig. 4. (A) Rate-dependent cyclic voltammograms of supercapacitor with ESM in 1 mol L^{-1} Na_2SO_4 aqueous solution at various scan rates (5–100 mV s^{-1}). (B) Cyclic voltammograms of supercapacitors with ESM and PP separators in 1 mol L^{-1} Na_2SO_4 aqueous solution at the scan rates of 15 mV s^{-1}. (C) GCD curves of AC electrodes in 1 mol L^{-1} Na_2SO_4 aqueous solution at the charge–discharge current density of 0.5, 1, 2, 3, and 5 A g^{-1}. (D) GCD curves of supercapacitors with ESM and PP separators in 1 mol L^{-1} Na_2SO_4 aqueous solution at the charge–discharge current density of 0.5 A g^{-1}.

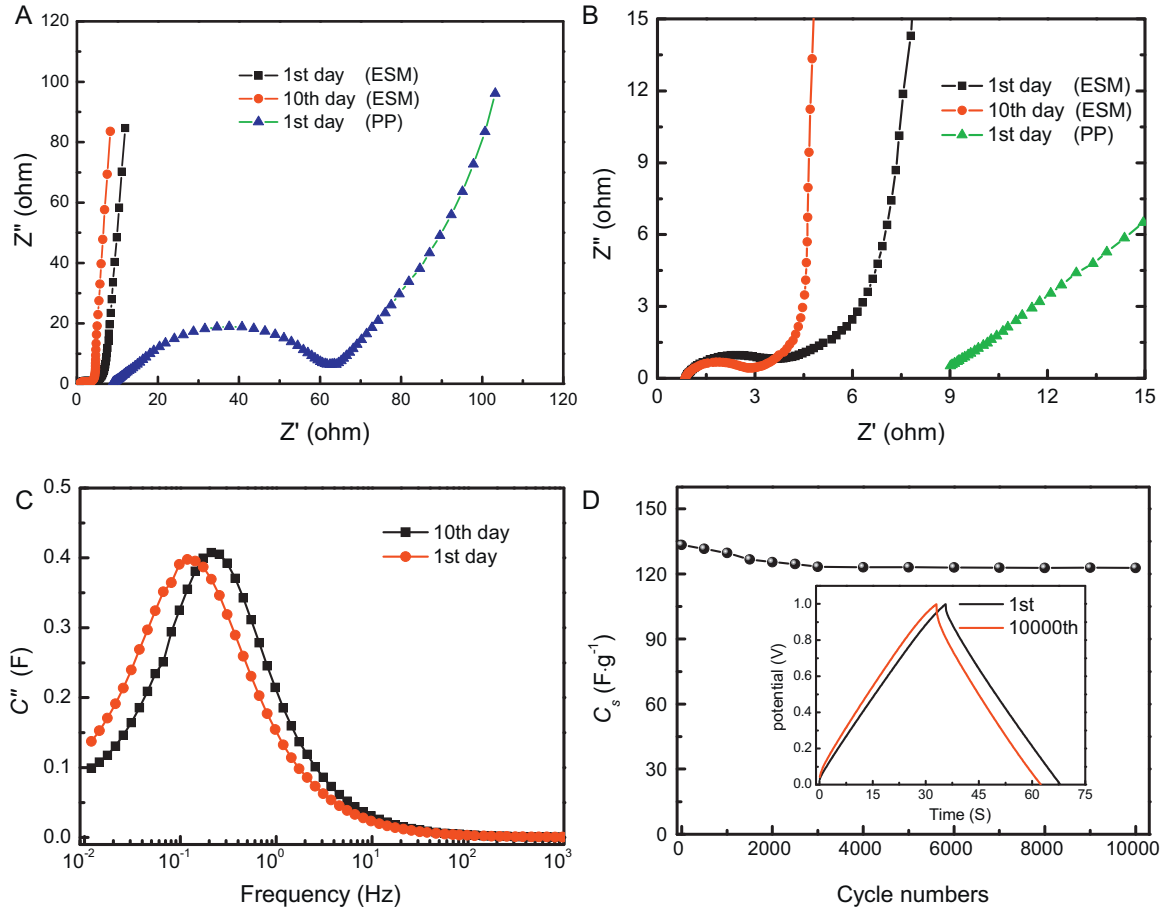

Fig. 5. (A) Complex plane impedance plots (Nyquist plots) of supercapacitors employing ESM and PP separators. (B) The close-up view of Nyquist plots in high-frequency region. (C) The evolution of the C' vs. the f of supercapacitor based on ESM separator. (D) Long-term cycling performance of supercapacitor employing ESM separator; insets show the GCD curves at 1st and 10,000th cycle.

ESM separator has better properties than the conventional separator.

Current density is one of the important factors, which directly characterize the capacitive behavior of the supercapacitor. The GCD curves of the supercapacitor at different current densities and potential range of 0–1 V using ESM as separator were shown in Fig. 4B. We can see that the charging curves are highly linear and symmetric with their corresponding discharge counterparts at various current densities from 0.5 to 5 A g^{-1}. This implies that the supercapacitor employing ESM separator has excellent electrochemical reversibility and charge–discharge properties [32]. The voltage loss (iR_{drop}) after a full charge is a measure of evaluating the equivalent series resistance (ESR) of the supercapacitor system [33]. Notably, the iR_{drop} are similar and not obvious, even at a high current density of 5 A g^{-1}, indicating little ESR and excellent capacitive properties of this supercapacitor system. From the GCD curves, the C_s of supercapacitor is calculated according to the Eq. (3) at different current density, as listed in Table 2. As can be seen, at a high current density of 5 A g^{-1}, the C_s maintains 90.91% of the values at low current density, demonstrating the good rate capability of supercapacitor using ESM separator once again.

Table 2
The C_s and η of the supercapacitor with ESM separator at different current densities.

Current density (A g^{-1})	1	2	3	5
C_s (F g^{-1})				
Charge	147.03	137.16	132.74	126.04
Discharge	133.40	127.73	126.11	121.28
η (%)	90.07	93.12	95.00	96.23

The coulombic efficiency (η), which is the ratio of charging capacitance to the discharge capacitance is another important parameter associated with the charge–discharge behavior of the supercapacitors [34]. The η evaluated from Eq. (4) has been observed to be close to 100% for each current density. It is worthwhile to note that the η increases smoothly with the increase of current density, indicating the good charge–discharge efficiency of supercapacitor employing ESM separator at high current density.

As comparison, the GCD measurements of supercapacitor based on conventional PP separator were determined and the results were presented in Fig. 4D. Obviously, the iR_{drop} of supercapacitor based on PP separator is about 0.3 V, which is much larger than the iR_{drop} of supercapacitor employing ESM separator (0.2 V). Due to the low wettability of PP membrane, a large part of capacity was exhausted by the inner resistance. Consequently, the output capacity is smaller than the one with ESM membrane. From the discussion above, we can infer that the ESM can be as a potential separator for the application of supercapacitor.

The EIS analysis has been recognized as one of the principal methods to examine the fundamental behaviors of supercapacitors [4,35]. Nyquist plots of the supercapacitor using ESM (the 1st day and 10th days) and PP separators (1st day) were measured in the frequency range of 10 mHz to 100 kHz with an AC perturbation of 5 mV were shown in Fig. 5A and B. From the close-up view of the left plot in high-frequency region, we can observe that the solution resistance (R_s, the intercept between the impedance plot and

the real impedance (Z') axis) of the supercapacitor do not change nearly, which still remain at a low value of 0.32 (cm^2. But the charge transfer resistance (R_{ct}, the span of the single semi-circle along the *X*-axis from high to low frequency) has a little increase compared to the original state, which may be resulted from the water uptake of ESM. At low frequency region, the Nyquist plots lines of the supercapacitor are still closed to parallel with the *Y*-axis, indicating good capacitive behaviors of supercapacitor after long-time storage. Clearly, the R_s and R_{ct} of supercapacitor employing PP separator are much large than that ones of supercapacitor with ESM separator, which implies the better properties of ESM separator.

The imaginary part (C'') of the capacitance vs. the frequency of supercapacitors using ESM separator were shown in Fig. 4B. Imaginary part of the complex capacitance corresponds to the dielectric loss of the electrolyte occurring during rotation or movement of the molecules of electrolyte [36]. Both of the plots go through a maximum at a particular frequency f_0. This frequency determines the dielectric relaxation time (τ), which is key factor of supercapacitor. The smaller value represents the less time of supercapacitor reach the half of the low frequency capacitance, implying the better characteristic of the whole system. It can be seen that the frequency at which peak maxima occur shifts to higher frequency when the supercapacitor was stored for a long time. Ten days later, the f_0 reaches to 0.21 Hz (the τ is 4.76 s), which indicates that the natural ESM is a superior separator material for the application of supercapacitor.

Moreover, cyclic durability is one of the most important electrochemical properties of supercapacitor. Fig. 4C shows the results of long-term cycling tests at a current density of 1 A g^{-1}, which suggest a capacitance retention of ≈92% compared to the original values after 10,000 charge–discharge cycles. The good cycling stability of the supercapacitor presented here illustrates that the ESM is stable and efficient for the application of supercapacitor separator.

4. Conclusions

In the current work, a natural and hierarchically ordered macroporous ESM was explored to act as the separator of supercapacitor. The favorable porous structures, high decomposition temperature (over 200 °C), low swelling degree, and good mechanical strength of ESM make ESM potential use in current commercial supercapacitors (<100 °C), and even in high-temperature supercapacitor (>100 °C). Furthermore, it can be concluded that ESM could be the best candidate for separator from the excellent electrochemical performances of supercapacitor, such as low resistance, quick charge–discharge ability (τ is 4.76 s) and outstanding cycling stability (92% retention after 10,000 cycles). We believe that the outstanding results presented here may pave the way for successfully exploring a high-efficient, low-cost, and stable biologic separator for supercapacitors and other applications.

Acknowledgments

This work was supported by the National High Technology Research and Development Program of China (No. 2009AA03Z217), the National Natural Science Foundation of China (Nos. 90922028, 50842027) and the Key Project of Chinese Ministry of Education (No. 211204).

References

[1] M. Inagaki, H. Konnoa, O. Tanaikeb, J. Power Sources 195 (2010) 7880.
[2] Z. Yang, J. Zhang, M. Kintner-Meyer, X. Lu, D. Choi, J.P. Lemmon, J. Liu, Chem. Rev. 111 (2011) 3577.
[3] L. Nyholm, G. Nyström, A. Mihranyan, M. Strømme, Adv. Mater. 23 (2011) 3751.
[4] A. Lasia, Electrochemical impedance spectroscopy and its applications, in: B.E. Conway, J. Bockris, R.E. White (Eds.), Modern Aspects of Electrochemistry, vol. 32, Kluwer Academic/Plenum Publishers, New York, 1999, pp. 143–248.
[5] E. Frackowiak, Phys. Chem. Chem. Phys. 9 (2007) 1774.
[6] M. Armand, F. Endres, D. MacFarlane, H. Ohno, B. Scrosati, Nat. Mater. 8 (2009) 621.
[7] P. Hall, M. Mirzaeian, S. Fletcher, F. Sillars, A. Rennie, G.O. Shitta-Bey, G. Wilson, A. Cruden, R. Carter, Energy Environ. Sci. 3 (2010) 1238.
[8] M. Winter, R.J. Brodd, Chem. Rev. (2004) 4245.
[9] S. Mayer, J. Kaschmitter, R. Pekala, US Patent 5,042,306 (1995).
[10] J. Day, C. Wei, US Patent 6,084,767 (2000).
[11] J. Yang, H. Wang, C. Yang, J. Membr. Sci. 322 (2008) 74.
[12] Y. Yin, O. Yamada, Y. Suto, T. Mishima, K. Tanaka, H. Kita, K. Okamoto, J. Polym. Sci. A: Polym. Chem. 43 (2005) 1545.
[13] J. Elliott, S. Paddison, Phys. Chem. Chem. Phys. 9 (2007) 2602.
[14] B. Choi, J. Hong, W. Hong, P. Hammond, H. Park, ACS Nano 5 (2011) 7205.
[15] J. Zhou, J. Cai, S. Cai, X. Zhou, A. Mansour, J. Power Sources 196 (2011) 10479.
[16] P. Staiti, F. Lufrano, Electrochim. Acta 55 (2010) 2436.
[17] J. Dennis, D. Carrino, K. Yamashita, A. Caplan, Matrix Biol. 19 (2000) 683.
[18] D. Yang, L. Qi, J. Ma, Adv. Mater. 14 (2002) 1543.
[19] D. Yang, L. Qi, J. Ma, J. Mater. Chem. 13 (2003) 1119.
[20] Q. Tang, J. Wu, Z. Tang, Y. Li, J. Lin, M. Huang, J. Mater. Chem. 21 (2011) 13354.
[21] Y. Amamoto, M. Kikuchi, H. Masunaga, H. Ogawa, S. Sasaki, H. Otsuka, A. Takahara, Polym. Chem. 2 (2011) 957.
[22] G. Lota, G. Milczarek, Electrochem. Commun. 13 (2011) 470.
[23] L. Demarconnay, E. Raymundo-Pinero, F. Béguin, Electrochem. Commun. 12 (2010) 1275.
[24] H. Yu, J. Wu, L. Fan, K. Xu, X. Zhong, Y. Lin, J. Lin, Electrochim. Acta 56 (2011) 6881.
[25] D. Hulicova-Jurcakova, A. Puziy, O. Poddubnaya, F. Suarez-García, J. Tascon, G. Lu, J. Am. Chem. Soc. 131 (2009) 5026.
[26] C. Meng, C. Liu, L. Chen, C. Hu, S. Fan, Nano Lett. 10 (2010) 4025.
[27] J. Wang, Y. Zhang, H. Wu, L. Xiao, Z. Jiang, J. Power Sources 195 (2010) 2526.
[28] F. Yi, Z. Guo, L. Zhang, J. Yu, Q. Li, Biomaterials 25 (2004) 4591.
[29] J. Golebiewski, A. Galeski, Compos. Sci. Technol. 67 (2009) 3442.
[30] E. Kontou, P. Farasoglou, J. Mater. Sci. 33 (1998) 147.
[31] S. Kundu, L. Simon, M. Fowler, S. Grot, Polymer 46 (2005) 11707.
[32] G. Ning, Z. Fan, G. Wang, J. Gao, W. Qian, F. Wei, Chem. Commun. 47 (2011) 5976.
[33] Q. Li, K. Li, C. Sun, Y. Li, J. Electroanal. Chem. 611 (2007) 43.
[34] K. Hirano, H. Yamato, K. Kunimoto, M. Ohwa, Anal. Chim. Acta 443 (2001) 265.
[35] I. Kovalenko, D.G. Bucknall, G. Yushin, Adv. Funct. Mater. 20 (2010) 3979.
[36] P. Taberna, P. Simon, J. Fauvarque, J. Electrochem. Soc. 150 (2003) A292.